Dalton Transactions

ROYAL SOCIETY OF CHEMISTRY

PAPER

View Article Online
View Journal | View Issue

Cite this: *Dalton Trans.*, 2022, **51**, 13094

The effects of introducing terminal alkenyl substituents into the 2,2′-bipyridine domain in $[Cu(N\hat{}N)(P\hat{}P)]^+$ coordination compounds†‡

Jannika Wöhler, Marco Meyer, Alessandro Prescimone, Catherine E. Housecroft * and Edwin C. Constable

The N^N chelating ligands 6,6′-bis(but-3-en-1-yl)-2,2′-bipyridine (**1**), 6-(but-3-en-1-yl)-6′-methyl-2,2′-bipyridine (**2**), 6,6′-bis(pent-4-en-1-yl)-2,2′-bipyridine (**3**) and 6-(pent-4-en-1-yl)-6′-methyl-2,2′-bipyridine (**4**) have been prepared, characterized, and incorporated into the heteroleptic $[Cu(N\hat{}N)(P\hat{}P)][PF_6]$ complexes in which P^P is either POP (bis(2-(diphenylphosphanyl)phenyl)ether) or xantphos (9,9-dimethyl-9*H*-xanthene-4,5-diyl)bis(diphenylphosphane). The eight coordination compounds have been fully characterized, including the single crystal structures of [Cu(**1**)(xantphos)][PF_6], [Cu(**1**)(POP)][PF_6]·CH_2Cl_2, [Cu(**2**)(xantphos)][PF_6], [Cu(**2**)(POP)][PF_6] and [Cu(**3**)(POP)][PF_6]·0.5Et_2O. The $[Cu(N\hat{}N)(P\hat{}P)]^+$ cations exhibit a partially reversible or irreversible Cu^+/Cu^{2+} oxidation at more positive potentials than the benchmark $[Cu(bpy)(P\hat{}P)]^+$ and $[Cu(Me_2bpy)(P\hat{}P)]^+$ complexes consistent with the increase in steric hindrance of the terminal alkenyl substituents. When excited in the region of the metal-to-ligand charge transfer (MLCT) absorption, solutions of the $[Cu(N\hat{}N)(P\hat{}P)][PF_6]$ complexes are weak emitters with λ_{em}^{max} in the range 565–578 nm. However, powdered samples achieve photoluminescence quantum yields in the range of 28.5 to 62.3%, with the highest PLQY found for [Cu(**3**)(POP)][PF_6] with an excited-state lifetime, τ, of 16.1 μs. For [Cu(**3**)(POP)][PF_6], the excited state lifetime was measured in MeTHF at 293 and 77 K, and the increase in τ from 1.77 to 59.4 μs upon cooling supports thermally activated delayed fluorescence (TADF) at ambient temperatures.

Received 8th June 2022,
Accepted 29th July 2022

DOI: 10.1039/d2dt01799g

rsc.li/dalton

Introduction

The current interest in the emissive behaviour of heteroleptic copper(I) coordination compounds stems from the influential work of McMillin and coworkers over 40 years ago. In 1978, Buckner and McMillin found that excitation into the metal-to-ligand charge transfer (MLCT) bands of $[Cu(bpy)(PPh_3)_2]^+$ (bpy = 2,2′-bipyridine) resulted in photoluminescence (PL) from low-lying charge transfer excited states.[1] Further investigations provided insight into the emission behaviour of $[Cu(N\hat{}N)_2]^+$ and $[Cu(N\hat{}N)(P\hat{}P)]^+$ complexes in which N^N is a diimine (typically a derivative of bpy or 1,10-phenanthroline, phen) and P^P is a chelating bis(phosphane).[2–7] An important advance was the observation that $[Cu(2,9\text{-}Me_2phen)_2]^+$ (2,9-Me_2phen = 2,9-dimethyl-1,10-phenanthroline) exhibited a long-lived emission in solution at room temperature.[5] A later development was the recognition that certain families of copper(I) complexes, including $[Cu(N\hat{}N)(P\hat{}P)]^+$ species, could exhibit thermally activated delayed fluorescence (TADF).[8–11] This phenomenon relies upon the energy gap between the singlet and triplet excited states (S_1 and T_1) being very small (≤0.12 eV).[8] Following photoexcitation from the singlet ground-state ($S_0 \rightarrow S_1$), inter-system crossing occurs to populate the T_1 state. With a sufficiently long T_1 lifetime, reverse intersystem crossing occurs, repopulating the S_1 state with subsequent singlet-emission. A motivation for enlarging the pool of available $[Cu(N\hat{}N)(P\hat{}P)]^+$ complexes is the development of efficient emissive materials for applications in light-emitting devices such as light-emitting electrochemical cells (LECs). In the device,

Department of Chemistry, University of Basel, Mattenstrasse 24a, BPR 1096, 4058 Basel, Switzerland. E-mail: catherine.housecroft@unibas.ch

†We dedicate this paper to Paul R. Raithby on the occasion of his 70th birthday. In addition to his devoted contributions to the chemical community, Paul has been a good friend and colleague to two of the authors for almost 40 years – from first mutual fumblings with the Cambridge Crystallographic Database, through acting as best man at our wedding to his present role as elder statesman in the UK crystallographic community. It has been a fun journey – thank you Paul.

‡Electronic supplementary information (ESI) available: Instrumentation; Fig. S1–S60: NMR spectra; Fig. S61–S65: structural figures; Fig. 66: cyclic voltammograms; Fig. S67: solution absorption spectra; Fig. S68–S69: excited state lifetime plots; Table S1: crystallographic data; Table S2: selected bond parameters; Table S3: components for second-order lifetime fits. CCDC 2171124–2171128. For ESI and crystallographic data in CIF or other electronic format see DOI: https://doi.org/10.1039/d2dt01799g

recombination of holes and electrons produces excitons in either a triplet (75%) or singlet (25%) state. It follows that, with a spin-forbidden $T_1 \rightarrow S_0$ decay, the internal quantum efficiency is restricted to 25%. Thus, for copper(I) emitters, TADF is critically important since it negates the requirement of spin–orbit coupling for mixing of triplet and singlet states.

$[Cu(N^N)(P^P)]^+$ complexes represent the largest family of emissive copper(I) complexes studied to date. Large-bite angle bis(phosphane) ligands are beneficial, and the commercially available POP and xantphos (Scheme 1) are the most popular. Introducing sterically-demanding substituents into the 6,6′-positions of bpy or 2,9-positions of phen has a highly beneficial effect on the PL behaviour.[12,13] This follows from the fact that photoexcitation formally oxidizes Cu(I) to Cu(II), causing flattening of the tetrahedral Cu(I) coordination geometry towards square-planar Cu(II). Steric protection of the metal atom mitigates against attack by solvent molecules to give a 5-coordinate exciplex with associated emission quenching. However, it has been observed that the presence of sterically-demanding groups may affect compound stability in solution with respect to dynamic ligand exchange.[14]

Overviews of $[Cu(N^N)(P^P)]^+$ emitters[10,11] reveal that some of the most efficient copper-based LECs have been fabricated using $[Cu(6,6'\text{-}Me_2bpy)(xantphos)][PF_6]$,[15] $[Cu(4,5,6\text{-}Me_3bpy)(xantphos)][PF_6]$,[16] and $[Cu(4,4'\text{-}(CF_3)_2\text{-}6,6'\text{-}Me_2bpy)(xantphos)][PF_6]$.[17] Compounds for which high values of the solid-state photoluminescence quantum yields (PLQYs) have been found include $[Cu(4,4',6,6'\text{-}Me_4bpy)(POP)][BF_4]$ (55% or 74%, depending on whether the sample was ground),[18] $[Cu(6\text{-}Mebpy)(xantphos)][PF_6]$ (34%),[15] $[Cu(6\text{-}Etbpy)(xant\text{-}phos)][PF_6]$ (37%),[15] and $[Cu(6,6'\text{-}Me_2bpy)(xantphos)][PF_6]$ (37%[15] or 62%,[19] the difference again being attributed to sample morphology). Although we recently demonstrated that the introduction of long and potentially sterically demanding 6-substituents into the bpy domain was not detrimental to the photophysical properties,[20] it appears that few investigations have considered substituents longer than an ethyl chain. In this work, we report the preparation and properties of $[Cu(N^N)(xantphos)][PF_6]$ and $[Cu(N^N)(POP)][PF_6]$ compounds in which the N^N ligands are **1–4** (Scheme 2). The ligand design aimed to address the effects of introducing long chain substituents, as well as allowing a comparison of asymmetrical and symmetrical substituent patterns. In addition, the introduction of the terminal alkene functionality provides a functional group that can be exploited for future ligand modifications.

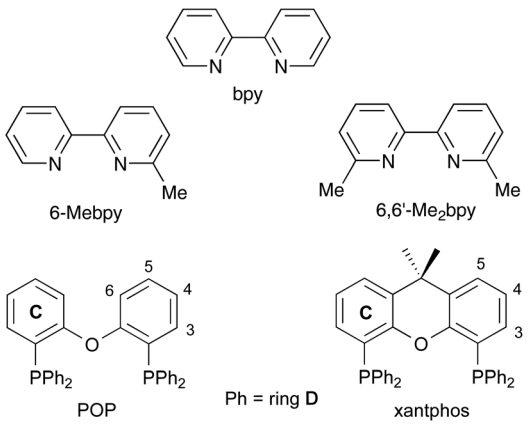

Scheme 1 Structures of 2,2′-bipyridine, 6-methyl-2,2′-bipyridine, 6,6′-dimethyl-2,2′-bipyridine, and of the P^P ligands with numbering for spectroscopic assignments.

Results and discussion

Synthesis of ligands 1–4

The four new ligands shown in Scheme 2 were prepared by adapting a previously reported procedure.[21] Initially, Me_2bpy was deprotonated using lithium diisopropylamide (LDA) in THF at −78 °C. This was followed by alkylation with the appropriate bromoalkene. For the preparation of ligand **1**, two equivalents of LDA and two equivalents of allyl bromide were used, while the preparation of ligand **2** only required one equivalent of both reagents. Compounds **1** and **2** were obtained in yields of 28% and 76%, respectively, after purification. When reacting Me_2bpy with two equivalents of LDA and two equivalents of 4-bromobut-1-ene, both ligands **3** and **4** were formed and were separated by column chromatography. Both ligands were obtained with yields of 27%.

The base peaks of the high resolution electrospray (HR-ESI) mass spectra appeared at *m*/*z* 265.17 for ligand **1**, 225.14 for **2**, 293.20 for **3** and 239.15 for **4**, and were assigned to the $[M + H]^+$ ion of the respective ligand. The ^1H and $^{13}C\{^1H\}$ NMR spectra were measured at room temperature in acetone-d_6 solutions and were assigned using COSY, NOESY, HMQC and HMBC methods with the atom labelling used for the assignments shown in Scheme 2. NMR and IR spectroscopic and mass spectrometric data for all ligands are shown in Fig. S1–

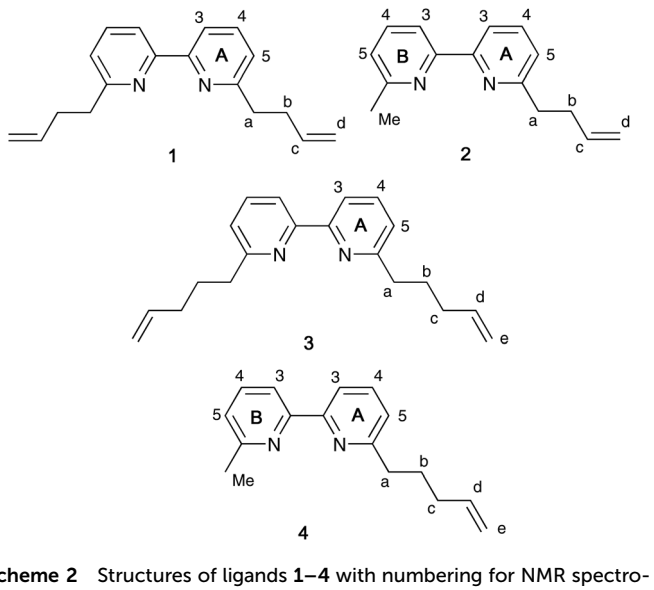

Scheme 2 Structures of ligands **1–4** with numbering for NMR spectroscopic assignments.

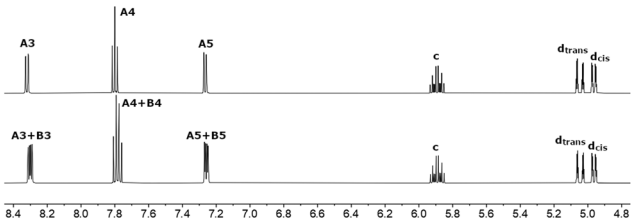

Fig. 1 Part of the 500 MHz ^{1}H NMR spectra of ligands **1** (top) and **2** (bottom) in acetone-d_6. Chemical shifts in δ/ppm. See Fig. S3 and S8‡ for the complete spectra. Atom labels are defined in Scheme 2.

S20.‡ In the ^{1}H NMR spectra, one set of pyridine ring signals (H^{A3}, H^{A4} and H^{A5}, Scheme 2) is visible for the symmetric ligands **1** and **3**, as can be seen in Fig. 1. The mono-substituted ligands **2** and **4** show two sets of overlapping pyridine ring signals (A and B rings, Scheme 2) and one methyl signal at lower frequency. The protons of the terminal double bond(s) are displayed in Fig. 1 between 4.9 and 6.0 ppm.

Synthesis and characterization of [Cu(N^N)(P^P)][PF$_6$]

Two strategies were applied for the synthesis of the [Cu(N^N)(P^P)][PF$_6$] complexes to ensure the formation of the heteroleptic complex over the kinetically more favoured homoleptic [Cu(N^N)$_2$][PF$_6$] complex. The strategies have been discussed in detail in previous publications.[17,22,23] For the [Cu(N^N)(xantphos)][PF$_6$] complexes, xantphos and the bpy ligand were dissolved in CH_2Cl_2 and this solution was added to a solution of [Cu(MeCN)$_4$][PF$_6$]. The [Cu(N^N)(POP)][PF$_6$] complexes were prepared by adding a solution of POP and [Cu(MeCN)$_4$][PF$_6$] to a solution of the bpy ligand. After purification of the compounds by layer diffusion crystallization from CH_2Cl_2 with Et_2O as antisolvent, the complexes were isolated as yellow or light-orange crystalline solids in yields between 33 and 79%.

The positive mode ESI mass spectrum of each copper(I) complex displayed peaks arising from [Cu(N^N)(P^P)]$^+$ and either the [Cu(POP)]$^+$ or [Cu(xantphos)]$^+$ cation. ^{1}H, ^{13}C{^{1}H} and ^{31}P{^{1}H} NMR spectra were recorded at room temperature in acetone-d_6 solutions, and the ^{1}H and ^{13}C{^{1}H} NMR spectra were assigned using COSY, NOESY, HMQC and HMBC methods. Fig. 2 shows the aromatic regions of the ^{1}H NMR spectra of [Cu(**2**)(POP)][PF$_6$] and [Cu(**2**)(xantphos)][PF$_6$]. In the spectra of all [Cu(N^N)(POP)][PF$_6$] complexes, the D ring protons (see Scheme 1) appear as broad signals (see Fig. 2, top). This can be rationalized in terms of molecular dynamics in solution, the POP ligand being significantly more flexible than xantphos. The ESI contains HR-ESI-MS, FTIR, ^{1}H NMR and HMQC and HMBC spectra for all the complexes (Fig. S21–S60‡).

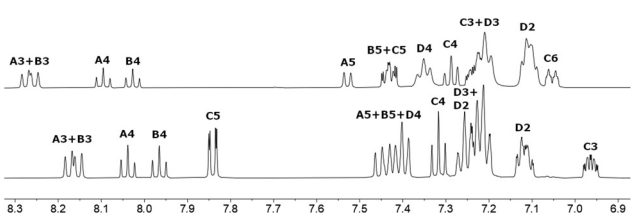

Fig. 2 Aromatic region of the 500 MHz ^{1}H NMR spectra of complexes [Cu(**2**)(POP)][PF$_6$] (top) and [Cu(**2**)(xantphos)][PF$_6$] (bottom) in acetone-d_6. Chemical shifts in δ/ppm. See Fig. S33 and S38‡ for the complete spectra. Atom labels are defined in Schemes 1 and 2.

Structural characterizations

X-ray quality single crystals of [Cu(**1**)(xantphos)][PF$_6$], [Cu(**1**)(POP)][PF$_6$]·CH_2Cl_2, [Cu(**2**)(xantphos)][PF$_6$], [Cu(**2**)(POP)][PF$_6$] and [Cu(**3**)(POP)][PF$_6$]·0.5Et_2O were grown by slow diffusion of Et_2O into CH_2Cl_2 solutions of the compounds. The crystallographic data are summarized in Table S1,‡ and selected structural metrics are presented in Tables 2 and S2.‡ The molecular structures of the complex cations are shown in Fig. S61–S65‡ and Fig. 3 displays the structures in stick representations for clarity. [Cu(**1**)(POP)][PF$_6$]·CH_2Cl_2 and [Cu(**3**)(POP)][PF$_6$]·0.5Et_2O crystallized in the triclinic space group $P\bar{1}$, while [Cu(**2**)(xantphos)][PF$_6$], [Cu(**2**)(POP)][PF$_6$] and [Cu(**1**)(xantphos)][PF$_6$] crystallized in the monoclinic space group $P2_1/n$ or $P2_1/c$. All structures suffered from disorders which were modelled as detailed in the Experimental section. Only the major occupancy sites are considered in the discussion.

In each structure, the copper(I) centre is in a distorted tetrahedral coordination environment with both the diimine and the bis(phosphane) ligands bound to the copper(I) in a bidentate chelating mode. The angle between the N–Cu–N plane and the P–Cu–P plane is 90.0° for [Cu(**1**)(xantphos)][PF$_6$], while the biggest distortion from tetrahedral geometry is found for [Cu(**2**)(POP)][PF$_6$] (79.8°). The N–Cu–N chelating angles lie in a small range (78.50(8) to 79.5(1)°). The P–Cu–P chelating angle in [Cu(**1**)(xantphos)][PF$_6$] (115.65(2)°) is noticeably larger than in the other complexes (Table 1). The Cu–N bond lengths lie in

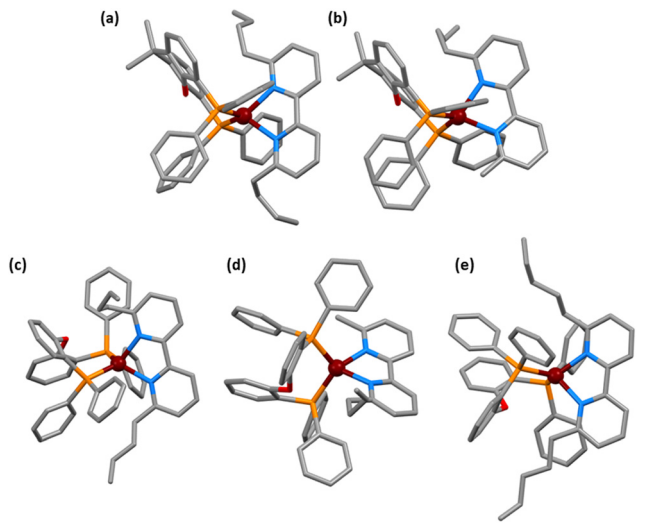

Fig. 3 The structures of the (a) [Cu(**1**)(xantphos)]$^+$, (b) [Cu(**2**)(xantphos)]$^+$, (c) [Cu(**1**)(POP)]$^+$, (d) [Cu(**2**)(POP)]$^+$ and (e) [Cu(**3**)(POP)]$^+$ cations. H atoms are omitted and only the major occupancy site is shown where there is disorder (see Experimental section). See Fig. S61 to S66‡ for thermal ellipsoids and atom labelling.

Table 1 Selected structural parameters within the cations in the [Cu(N^N)(P^P)][PF_6] compounds

Complex cation	P–Cu–P chelating angle/°	N–Cu–N chelating angle/°	P···P distance/Å	Angle between PCuP and NCuN planes/°	N–C–C–N torsion angle/°
[Cu(**1**)(xantphos)]$^+$	115.65(2)	78.94(8)	3.8874(8)	90.0	11.8(3)
[Cu(**1**)(POP)]$^+$	111.65(4)	79.5(1)	3.784(1)	81.2	13.9(5)
[Cu(**2**)(xantphos)]$^+$	111.36(3)	78.50(8)	3.8090(9)	86.6	−18.9(3)
[Cu(**2**)(POP)]$^+$	111.94(4)	79.2(1)	3.789(1)	79.8	−12.0(5)
[Cu(**3**)(POP)]$^+$	111.75(3)	79.3(1)	3.778(1)	81.9	−13.0(5)

a range of 2.104(3) to 2.156(2) Å and the Cu–P bond lengths vary between 2.280(1) and 2.3174(7) Å. The geometry of the bpy domain can be analysed by looking at the N–C–C–N torsion angle which has values ranging from 11.8(3)° for [Cu(**1**)(xantphos)]$^+$ to −18.9(3)° for [Cu(**2**)(xantphos)]$^+$.

All POP-containing structures exhibit offset face-to-face π-stacking interactions between one phenyl ring of the POP backbone and one of the phenyl rings in a PPh_2 unit (Fig. 4). The centroid···centroid distances between the stacked rings is 3.55 Å for [Cu(**2**)(POP)][PF_6], 3.71 Å for [Cu(**3**)(POP)][PF_6] and 3.80 Å for [Cu(**1**)(POP)][PF_6]. The angle between the least squares planes through the two stacked rings is 10.4° for [Cu(**2**)(POP)][PF_6], 14.1° for [Cu(**3**)(POP)][PF_6] and 19.7° for [Cu(**1**)(POP)][PF_6]. Although this last angle is somewhat large, the interactions correspond to the definitions of offset, parallel displaced π-stacking interactions described by Janiak.[24]

For [Cu(**1**)(xantphos)][PF_6] and [Cu(**2**)(xantphos)][PF_6], the xanthene backbone of the bisphosphane ligand favours a boat conformation to minimize strain. The 'bowl' shaped cavity of the xanthene unit accommodates one of the alkenyl substituents of the diimine ligand as shown in Fig. 5. We note that all three of the complexes containing 6,6′-disubstituted bpy ligand exhibit one disordered alkenyl substituent, indicating that the alkyl chain can adopt different conformations in the solid state.

Electrochemistry

The electrochemical properties of the [Cu(N^N)(P^P)][PF_6] complexes were investigated by cyclic voltammetry. The measurements were performed in dry CH_2Cl_2 solutions of the complexes with *ca.* 0.1 mol dm^{-3} [^{n}Bu$_4$N][PF_6] as supporting electrolyte. The cyclic voltammograms (CVs) of the complexes

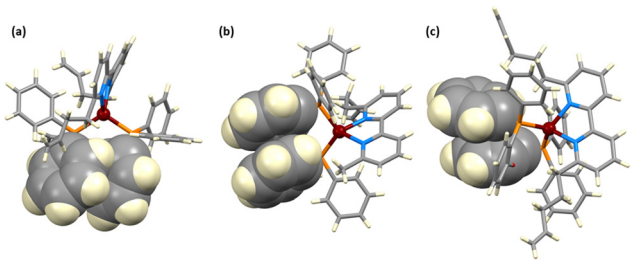

Fig. 4 Offset face-to-face π-stacking of one POP backbone ring with one phenyl ring of one diphenylphosphane unit in (a) [Cu(**1**)(POP)][PF_6], (b) [Cu(**2**)(POP)][PF_6] and (c) [Cu(**3**)(POP)][PF_6]. Only major occupancies are shown.

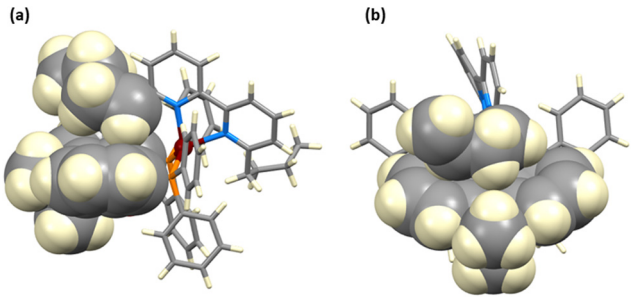

Fig. 5 Accommodation of an alkenyl substituent from ligands **1** and **2** within the xantphos 'bowl' created by the xanthene backbone in (a) [Cu(**1**)(xantphos)][PF_6] and in (b) [Cu(**2**)(xantphos)][PF_6]. Only major occupancies are shown.

are shown in Fig. S66,‡ and the potentials of the oxidative and reductive processes are given in Table 2. The table also gives data for benchmark complexes containing either bpy or Me_2bpy for comparison. All potentials were internally referenced to ferrocene (Fc/Fc^+).

The xantphos containing complexes all show a partially reversible oxidative process between $^{ox}_{1/2}$ = +0.92 and +0.95 V, that is assigned to the Cu^+/Cu^{2+} oxidation. This process was found to be irreversible for the POP complexes, with E_{pa} values

Table 2 Cyclic voltammetric data for the [Cu(N^N)(P^P)][PF_6] complexes and benchmark compounds referenced to internal Fc/Fc^+ = 0.0 V; CH_2Cl_2 (dry) solutions with [^{n}Bu$_4$N][PF_6] as supporting electrolyte and scan rate of 0.1 V s^{-1}. When the oxidative process is reversible, both $^{ox}_{1/2}$ and $E_{pa} - E_{pc}$ are given. For an irreversible process, only E_{pa} or E_{pc} is given

Complex cation	Oxidative process			Reductive process
	$E^{ox}_{1/2}$/V	$E_{pa} - E_{pc}$/mV	E_{pa}	E_{pc}/V
[Cu(bpy)(xantphos)]$^+$ [a]	+0.76	110		
[Cu(bpy)(POP)]$^+$ [a]	+0.72	110		
[Cu(Me_2bpy)(xantphos)]$^+$ [b]	+0.89	145		
[Cu(Me_2bpy)(POP)]$^+$ [b]	+0.92	183		
[Cu(**1**)(xantphos)]$^+$	+0.94	140		−2.32
[Cu(**1**)(POP)]$^+$			+0.96	−2.23
[Cu(**2**)(xantphos)]$^+$	+0.92	120		−2.35
[Cu(**2**)(POP)]$^+$			+0.97	−2.24
[Cu(**3**)(xantphos)]$^+$	+0.93	150		−2.41
[Cu(**3**)(POP)]$^+$			+0.96	−2.25
[Cu(**4**)(xantphos)]$^+$	+0.95	190		−2.35
[Cu(**4**)(POP)]$^+$			+0.95	−2.31

[a] Data from ref. 17. [b] Data from ref. 16.

between +0.95 and +0.97 V. When comparing these results to the potentials measured for [Cu(bpy)(P^P)][PF_6] and [Cu(Me_2bpy)(P^P)][PF_6] (Table 2), the oxidation potential moves to higher potential as 6 and 6′-substituents are introduced and as the size of the substituent increases. As the Cu^+/Cu^{2+} oxidation is associated with a change in geometry from tetrahedral to square-planar, the higher oxidation potentials can be justified by the steric hindrance of the 6- and 6′-substituents which inhibits the flattening of the coordination sphere.[16] This phenomenon is similar to the trend found for the introduction of 2,9-substituents into phen.[3,7,25] The data in Table 2 are consistent with the steric protection of the Cu(I) centre being enhanced upon going from Me_2bpy to ligands **1–4**. Note that, from the second cycle of the CV measurement onwards, an irreversible oxidation peak was observed at +0.66 V for the complexes (Fig. S66‡). This process may be attributed to an ECE process occurring during the first cycle. Each complex displays an irreversible ligand-centred reduction process with values of E_{pc} between −2.23 and −2.41 V (Table 2).

Photophysical properties

The absorption spectra of CH_2Cl_2 solutions of the copper(I) complexes exhibit intense, high-energy absorption bands below 330 nm arising from ligand-centred π* ← π transitions. In addition, a broad, lower intensity metal-to-ligand charge transfer (MLCT) band is visible with λ_{max} between 369 and 373 nm, consistent with previous absorption maxima for similar complexes.[11] The absorption data are given in Table 3 and the absorption spectra of the xantphos- and POP-containing complexes are shown in Fig. 6 and S67,‡ respectively. The maxima of the MLCT bands are similar for all the complexes containing ligands **1–4**, and inspection of Table 3 reveals a small blue shift with respect to the benchmark complexes containing bpy or Me_2bpy.[17,19] This is consistent with a greater σ-donating character of the alkyl chains compared to the methyl groups in Me_2bpy. The electron donation of the substituents destabilizes the LUMO of the complex which is located on the bpy ligand.[16]

The normalized solution and solid-state emission spectra of the complexes in deaerated CH_2Cl_2 solution are displayed in Fig. 7 and 8, and the corresponding emission data are summarized in Tables 4 and 5, respectively. All measurements were performed with an excitation wavelength (λ_{exc}) of 365 nm. Upon excitation, the CH_2Cl_2 solutions of the complexes emitted in the range λ_{em}^{max} = 565 nm for [Cu(**3**)(xantphos)][PF_6] to 578 nm for [Cu(**1**)(POP)][PF_6]. The solution spectra also display a lower energy shoulder at 620 nm, consistent with solution emission spectra of related [Cu(N^N)(P^P)][PF_6] complexes.[15,18,26–28] The xantphos containing complexes display a small blue-shift compared to the POP complexes in the solution emission. Powdered samples exhibited blue-shifted emission maxima (521 nm for [Cu(**1**)(POP)][PF_6] to 539 nm for [Cu(**4**)(POP)][PF_6]) compared to solution emissions.

A comparison of the emission data for complexes containing ligands **1–4** with data for benchmark complexes[16,17,27] shown in Tables 4 and 5 reveals a shift in the emission maxima to lower wavelengths with the longer-chain substituents. This is consistent with the trends in the electrochemical data.

The non-deaerated CH_2Cl_2 solutions of the complexes achieved PLQY values between 0.8 and 1.7% (Table 4).

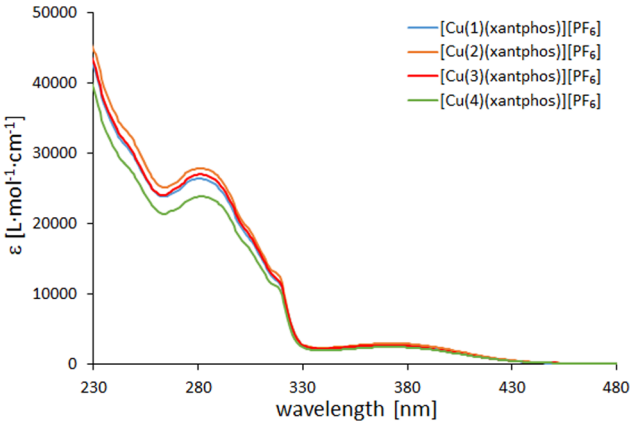

Fig. 6 Solution absorption spectra of the [Cu(N^N)(xantphos)][PF_6] complexes in dichloromethane (5 × 10^{-5} M).

Table 3 Solution absorption maxima for the [Cu(N^N)(P^P)][PF_6] complexes (CH_2Cl_2, 5.0 × 10^{-5} M)

	λ_{max}/nm (ε_{max}/dm^3 mol^{-1} cm^{-1})	
Complex cation	π* ← π	MLCT
[Cu(bpy)(xantphos)]$^+$ [a]		383
[Cu(bpy)(POP)]$^+$ [a]		388
[Cu(Me_2bpy)(xantphos)]$^+$ [b]	279 (26 700), 285 (26 500), 304 sh (18 200), 316 sh (12 200)	374 (2580)
[Cu(Me_2bpy)(POP)]$^+$ [b]	290 (18 200), 305 sh (16 400), 318 sh (12 000)	374 (2410)
[Cu(**1**)(xantphos)]$^+$	281 (26 444), 306 sh (17 328), 318 sh (11 784)	373 (2674)
[Cu(**1**)(POP)]$^+$	291 (20 298), 306 sh (18 760), 318 sh (13 736)	369 (2426)
[Cu(**2**)(xantphos)]$^+$	281 (27 942), 306 sh (18 418), 318 sh (12 818)	373 (2940)
[Cu(**2**)(POP)]$^+$	290 (21 872), 306 sh (19 902), 318 sh (14 628)	371 (2734)
[Cu(**3**)(xantphos)]$^+$	282 (27 034), 306 sh (17 794), 318 sh (12 034)	369 (2678)
[Cu(**3**)(POP)]$^+$	290 (20 422), 306 sh (18 996), 318 sh (14 054)	370 (2410)
[Cu(**4**)(xantphos)]$^+$	281 (23 896), 306 sh (15 810), 318 sh (10 956)	370 (2438)
[Cu(**4**)(POP)]$^+$	283 (19 668), 306 sh (17 786), 318 sh (13 060)	370 (2464)

[a] Data from ref. 17. [b] Data from ref. 19.

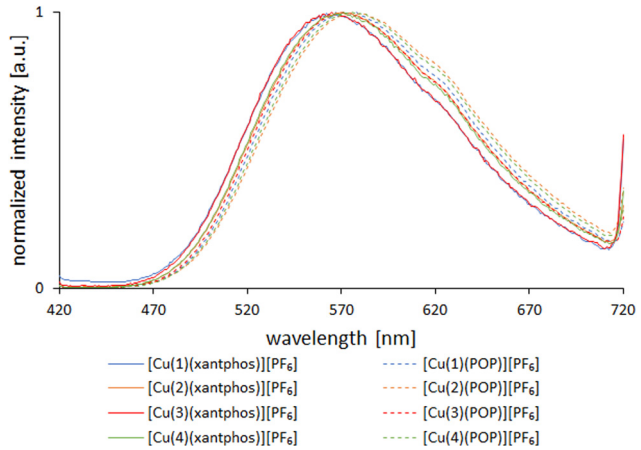

Fig. 7 Normalized solution emission spectra of [Cu(N^N)(P^P)][PF_6] complexes (1.0×10^{-5} M in dichloromethane with excitation at 365 nm).

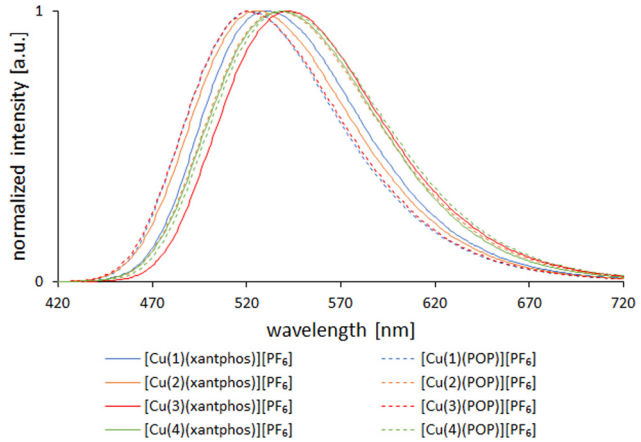

Fig. 8 Normalized powder emission spectra of [Cu(N^N)(P^P)][PF_6] complexes with excitation at 365 nm.

Table 4 Solution emission maxima, PLQY and excited state lifetime of the [Cu(N^N)(P^P)][PF_6] complexes (CH_2Cl_2, 2.5×10^{-5} M)

Complex cation	λ_{em}^{max}/nm	PLQY/% (non-deaer./deaer.)	τ/μs (non-deaer./deaer.)
[Cu(bpy)(xantphos)]$^{+}$ [a]	620	0.5/0.5	0.08/0.10
[Cu(bpy)(POP)]$^{+}$ [a]	618	0.4/0.5	0.04/0.05
[Cu(Me_2bpy)(xantphos)]$^{+}$ [a]	606	1.6/10.0	0.5/3.4
[Cu(Me_2bpy)(POP)]$^{+}$ [b]	564	1.3/13.8	0.3/4.0
[Cu(**1**)(xantphos)]$^{+}$	567	1.0/14.6	0.4/4.9
[Cu(**1**)(POP)]$^{+}$	578	1.1/17.7	0.4/5.4
[Cu(**2**)(xantphos)]$^{+}$	570	0.8/10.9	0.3/4.6
[Cu(**2**)(POP)]$^{+}$	575	1.0/16.3	0.3/5.3
[Cu(**3**)(xantphos)]$^{+}$	565	0.9/15.5	0.4/5.6
[Cu(**3**)(POP)]$^{+}$	571	1.7/20.0	0.4/5.4
[Cu(**4**)(xantphos)]$^{+}$	571	0.8/11.4	0.3/4.8
[Cu(**4**)(POP)]$^{+}$	576	1.0/16.7	0.3/5.0

[a] Data from ref. 17. [b] Data from ref. 26 and 15.

Table 5 Emission maxima, PLQY and excited state lifetime from a biexponential fit[a] of the [Cu(N^N)(P^P)][PF_6] complexes as powders

Complex cation	λ_{em}^{max}/nm	PLQY/%	$\langle\tau\rangle^{a}$/μs
[Cu(bpy)(xantphos)]$^{+}$ [b]	587	1.7	1.3
[Cu(bpy)(POP)]$^{+}$ [b]	581	3.0	1.5
[Cu(Me_2bpy)(xantphos)]$^{+}$ [b]	539	37.3	11.4
[Cu(Me_2bpy)(POP)]$^{+}$ [c]	535	43.2	10.5
[Cu(**1**)(xantphos)]$^{+}$	532	43.1	12.6
[Cu(**1**)(POP)]$^{+}$	521	60.5	15.1
[Cu(**2**)(xantphos)]$^{+}$	526	50.5	12.0
[Cu(**2**)(POP)]$^{+}$	537	38.4	12.2
[Cu(**3**)(xantphos)]$^{+}$	541	37.9	11.8
[Cu(**3**)(POP)]$^{+}$	522	62.3	16.1
[Cu(**4**)(xantphos)]$^{+}$	537	28.5	10.8
[Cu(**4**)(POP)]$^{+}$	539	35.4	12.7

[a] Components for the biexponential fit are given in Table S3.‡ [b] Data from ref. 17. [c] Data from ref. 26.

Deaerating the solutions with argon to prevent non-radiative quenching of the triplet excited state led to an enhancement of the emissive behaviour with PLQY values of 10.9% for [Cu(**2**)(xantphos)][PF_6] and 20.0% for [Cu(**3**)(POP)][PF_6] (Table 4). The PLQY values increased significantly on going from solution to powdered samples, with values in the range 28.5% for [Cu(**4**)(xantphos)][PF_6] to 62.3% for [Cu(**3**)(POP)][PF_6]. This trend is consistent with PLQY values for related heteroleptic copper(I) complexes and is due to the geometry change upon excitation which leads to non-radiative relaxation especially in solution.[18,29]

Overall the complexes with the 6,6′-disubstituted bpy ligands **1** and **3** performed better than the complexes with the asymmetric ligands **2** and **4**, and this is consistent with the increased steric hindrance of the substituents around the Cu(I) coordination sphere. This trend is supported by the data of the benchmark complexes with bpy and Me_2bpy ligands included in Tables 4 and 5.

The excited state lifetimes of the complexes in solution and in the solid-state are given in Tables 4 and 5. For the determination of the excited state lifetime $\langle\tau\rangle$ in the solid-state, a biexponential fit was used (see Table S3‡), while a monoexponential fit was used for solution data. In deaerated solutions, the excited state lifetimes range from 4.6 μs for [Cu(**2**)(xantphos)][PF_6] to 5.6 μs for [Cu(**3**)(xantphos)][PF_6], and increase for the powder samples, with the highest value being 16.1 μs for [Cu(**3**)(POP)][PF_6]. Consistent with the PLQY values, a trend is observed when comparing the excited state lifetimes with those of the benchmark complexes containing bpy and Me_2bpy (Tables 4 and 5). The substitution in 6 and 6′ position on the diimine ligand leads to longer excited state lifetimes due to the increased steric hindrance and stabilization of tetrahedral geometry.

Whether or not a material is a TADF emitter can be probed experimentally by comparing values of τ and λ_{em}^{max} at ambient and low temperatures. The emission spectrum and excited state lifetime of the best performing complex [Cu(**3**)(POP)][PF_6] were measured at room temperature (293 K) and 77 K in deaer-

Table 6 Solution emission maxima and excited state lifetime of [Cu(**3**)(POP)][PF_6] at room temperature (293 K) and at 77 K (MeTHF, 4.0×10^{-5} M, λ_{exc} = 355 nm)

Temperature/K	λ_{em}^{max}/nm	τ/μs
77	529	59.4
293	563	1.77

ated MeTHF (2-methyltetrahydrofuran). The results are summarized in Table 6 and the emission spectra are shown in Fig. 9. The two decay curves and their fits for the determination of the excited state lifetimes are shown in Fig. S68 and S69.‡ If the compound is a TADF emitter, we would expect to see a red-shift of the emission maximum upon cooling because of a switch from major contributions to the emission from $S_1 \rightarrow S_0$ (fluorescence) to $T_1 \rightarrow S_0$ (phosphorescence at 77 K). Instead, Fig. 9 shows a blue shift from 563 to 529 nm as the environment becomes more rigid. This rigidochromic effect is found in charge-transfer emission bands in rigid media, although it is not commonly found in heteroleptic copper(I) complexes.[29–32] The room temperature excited state lifetime of 1.77 μs of [Cu(**3**)(POP)][PF_6] in MeTHF compares with 5.43 μs measured in CH_2Cl_2 (Table 4). Upon cooling to 77 K, the value of τ is extended to 59.4 μs. The increase from 5.43 to 59.4 μs is similar to that seen for other [Cu(N^N)(POP)][PF_6] complexes,[11] and is consistent with phosphorescence being the principal decay pathway at low temperature. We consider this to be strong evidence for TADF behaviour as the low temperature pure radiative lifetime (estimated by the inverse of the decay rate constant) is higher than at room temperature, excluding explanations based on reduced non-radiative decay at 77 K.

Experimental

General

^{1}H, ^{13}C{^{1}H} and ^{31}P{^{1}H} NMR spectra were recorded at room temperature in acetone-d_6 using a Bruker Avance III-500 NMR spectrometer. ^{1}H and ^{13}C chemical shifts were referenced to residual solvent peaks (^{1}H δ(acetone-d_5) = 2.50 ppm, ^{13}C δ(acetone-d_6) = 29.8 ppm).

Absorption and emission spectra in solution were measured using a Shimadzu UV-2600 spectrophotometer and a Shimadzu RF-6000 spectrofluorometer, respectively. A Shimadzu LCMS-2020 instrument was used to record electrospray (ESI) mass spectra. Quantum yields (CH_2Cl_2 solution and powder) were measured using a Hamamatsu absolute photoluminescence (PL) quantum yield spectrometer C11347 Quantaurus-QY. Powder emission spectra and excited state lifetimes (in Tables 4 and 5) were measured with a Hamamatsu Compact Fluorescence Lifetime Spectrometer C11367 Quantaurus-Tau with an LED light source (λ_{exc} = 365 nm). Lifetimes were obtained by fitting the measured data to an exponential decay using MATLAB®; a biexponential fit was used when a single exponential fit gave a poor result. Where stated, the sample was deaerated using argon bubbling for 15 min. MeTHF solution and low temperature (77 K) emission spectra and excited-state lifetimes were measured using an LP920-KS instrument from Edinburgh Instruments. The excitation at 355 nm was performed by a frequency-tripled Nd:YAG laser (Quantel Q-smart 450 mJ, *ca.* 10 ns pulse width) with a beam expander (BE02-355 from Thorlabs). The typical pulse energy was 40 mJ at 355 nm. Lifetimes were obtained by fitting the measured data to an exponential decay using Origin®.

Electrochemical measurements used an AMETEK VersaSTAT 3F potentiostat (AMETEK Princeton Applied Research, Oak Ridge, United States) with [^{n}Bu$_4$N][PF_6] (0.1 M) as supporting electrolyte and a scan rate of 0.1 V s^{-1}; the solvent was dry CH_2Cl_2 and solution concentrations were *ca.* 2×10^{-3} mol dm^{-3}. The solutions were constantly deaerated with argon bubbling. The working electrode was glassy carbon, the reference electrode was a leakless Ag/AgCl (eDAQ ET069-1) and the counter-electrode was a platinum wire. Final potentials were internally referenced with respect to the Fc/Fc$^+$ couple.

[Cu(MeCN)$_4$][PF_6] was prepared according to a literature procedure.[1] 6,6′-Me$_2$-bpy was purchased from Fluorochem. 4-Bromo-1-butene and POP were bought from Acros Organics and allyl bromide and xantphos from Sigma Aldrich.

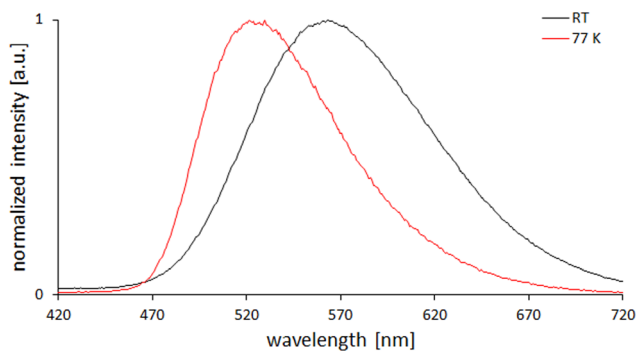

Fig. 9 Normalized solution emission spectra of [Cu(**3**)(POP)][PF_6] in deaerated MeTHF at room temperature and 77 K with excitation at 355 nm.

Synthetic procedures

Compound 1. Under a N_2 atmosphere, diisopropylamine (0.613 mL, 4.34 mmol, 2.0 eq.) was dissolved in 5 mL dry and deaerated THF, and *n*-butyllithium (2.5 M in hexanes, 1.74 mL, 4.34 mmol, 2.0 eq.) was added at −78 °C. The mixture was stirred for 1 h at −78 °C. A solution of 6,6′-dimethyl-2,2′-bipyridine (400 mg, 2.17 mmol, 1.0 eq.) in 10 mL dry and deaerated THF was added, and the mixture was stirred for 3 h at −78 °C. Then, allyl bromide (0.367 mL, 4.34 mmol, 2.0 eq.) was added to the reaction mixture in 10 mL dry and deaerated THF. The mixture was stirred and allowed to warm to room temperature overnight. The reaction was quenched by adding saturated NH_4Cl solution (15 mL) and the organic phase was extracted with CH_2Cl_2 (3 × 30 mL), dried over $MgSO_4$ and the solvent

was removed under reduced pressure. The residue was purified by silica column chromatography (2 to 9% ethyl acetate in cyclohexane) to yield **1** (161.7 mg, 0.612 mmol, 28%) as a colourless oil. ^{1}H NMR (500 MHz, acetone-d_6, 298 K) δ/ppm: 8.33 (dd, $^3J_{HH}$ = 7.8, $^4J_{HH}$ = 1.0 Hz, 2H, H^{A3}), 7.81 (dd, $^3J_{HH}$ = 7.7, 7.7 Hz, 2H, H^{A4}), 7.31–7.25 (m, 2H, H^{A5}), 5.94 (ddt, $^3J_{HH}$ = 16.9, 10.3, 6.6 Hz, 2H, H^c), 5.11–5.04 (m, 2H, H^d*$_{trans}$*), 4.96 (ddt, $^3J_{HH}$ = 10.2, $^2J_{HH}$ = 2.1 Hz, 2H, H^d*$_{cis}$*), 2.98–2.92 (m, 4H, H^a), 2.58 (tdt, $^3J_{HH}$ = 7.7, 6.6, $^2J_{HH}$ = 1.4 Hz, 4H, H^b). ^{13}C{^{1}H} NMR (126 MHz, acetone-d_6, 298 K) δ/ppm: 161.5 (C^{A6}), 156.5 (C^{A2}), 139.1 (C^c), 137.9 (C^{A4}), 123.7 (C^{A5}), 118.8 (C^{A3}), 115.2 (C^d), 38.1 (C^a), 34.2 (C^b). HR-ESI-MS: *m*/*z* 265.1702 [M + H]$^+$ (base peak, calc. 265.1699), 287.1514 [M + Na]$^+$ (calc. 287.1519).

Compound 2. Under a N_2 atmosphere, diisopropylamine (0.307 mL, 2.17 mmol, 1.0 eq.) was dissolved in 5 mL dry and deaerated THF, and *n*-butyllithium (2.5 M in hexanes, 0.868 mL, 2.17 mmol, 1.0 eq.) was added at −78 °C. The mixture was stirred for 1 h at −78 °C. A solution of 6,6′-dimethyl-2,2′-bipyridine (400 mg, 2.17 mmol, 1.0 eq.) in 10 mL dry and deaerated THF was added, and the mixture was stirred for 2 h at −78 °C. Then, allyl bromide (0.184 mL, 2.17 mmol, 1.0 eq.) was added to the reaction mixture in 10 mL dry and deaerated THF. The mixture was stirred and allowed to warm to room temperature overnight. The reaction mixture was quenched by adding saturated aqueous NH_4Cl solution (15 mL). The organic phase was extracted with CH_2Cl_2 (3 × 30 mL), dried over $MgSO_4$ and the solvent was removed under reduced pressure. The residue was purified by silica column chromatography (5 to 25% ethyl acetate in cyclohexane) to yield **2** (367.4 mg, 1.638 mmol, 76%) as a colourless oil. ^{1}H NMR (500 MHz, acetone-d_6, 298 K) δ/ppm: 8.35–8.26 (m, 2H, H^{A3+B3}), 7.79 (dt, $^3J_{HH}$ = 8.6, 7.8 Hz, 2H, H^{A4+B4}), 7.26 (ddd, $^3J_{HH}$ = 7.7, 6.4, $^4J_{HH}$ = 1.1 Hz, 2H, H^{A5+B5}), 5.94 (ddt, $^3J_{HH}$ = 16.9, 10.2, 6.6 Hz, 1H, H^c), 5.07 (dq, $^3J_{HH}$ = 17.2, $^4J_{HH}$ = 1.7 Hz, 1H, H^d*$_{trans}$*), 5.00–4.92 (m, 1H, H^d*$_{cis}$*), 2.98–2.91 (m, 2H, H^a), 2.63–2.54 (m, 5H, H^{b+Me}). ^{13}C{^{1}H} NMR (126 MHz, acetone-d_6, 298 K) δ/ppm: 161.5 (C^{A6}), 158.5 (C^{B6}), 156.5 (C$^{A2/B2}$), 156.4 (C$^{A2/B2}$), 139.1 (C^c), 137.9 (C$^{A4/B4}$), 137.9 (C$^{A4/B4}$), 123.9 (C$^{A5/B5}$), 123.6 (C$^{A5/B5}$), 118.8 (C$^{A3/B3}$), 118.5 (C$^{A3/B3}$), 115.2 (C^d), 38.1 (C^a), 34.2 (C^b), 24.6 (C^{Me}). HR-ESI-MS: *m*/*z* 225.1388 [M + H]$^+$ (base peak, calc. 225.1386).

Compound 3 and 4. Under a N_2 atmosphere, diisopropylamine (0.613 mL, 4.34 mmol, 2.0 eq.) was dissolved in 5 mL dry and deaerated THF and *n*-butyllithium (2.5 M in hexanes, 1.74 mL, 4.34 mmol, 2.0 eq.) was added at −78 °C. The mixture was stirred for 1 h at −78 °C. A solution of 6,6′-dimethyl-2,2′-bipyridine (400 mg, 2.17 mmol, 1.0 eq.) in 10 mL dry and deaerated THF was added, and the mixture was stirred for 3 h at −78 °C. Then, 4-bromo-1-butene (0.441 mL, 4.34 mmol, 2.0 eq.) was added to the reaction mixture in 10 mL dry and deaerated THF. The mixture was stirred and allowed to warm to room temperature overnight. The reaction was quenched by adding saturated NH_4Cl solution (15 mL) and the organic phase was extracted with CH_2Cl_2 (3 × 30 mL), dried over $MgSO_4$ and the solvent was removed under reduced pressure. The residue was purified by silica column chromatography (3 to 15% ethyl acetate in cyclohexane) to yield **3** (169 mg, 0.58 mmol, 27%) and **4** (173 mg, 0.59 mmol, 27%) as colourless oils in different fractions (with the disubstituted product **3** in the first and the mono-substituted **4** in the second fraction). Compound **3**: ^{1}H NMR (500 MHz, acetone-d_6, 298 K) δ/ppm: 8.32 (dd, ^3J = 7.8, ^4J = 1.0 Hz, 2H, H^{A3}), 7.80 (t, ^3J = 7.7 Hz, 2H, H^{A4}), 7.27 (dd, ^3J = 7.7, ^4J = 1.0 Hz, 2H, H^{A5}), 5.89 (ddt, ^3J = 17.0, 10.2, 6.7 Hz, 2H, H^d), 5.05 (ddt, ^3J = 17.1, ^2J = 1.6 Hz, 2H, H^e*$_{trans}$*), 4.96 (ddt, ^3J = 10.2, 2.3, ^2J = 1.2 Hz, 2H, H^e*$_{cis}$*), 2.91–2.84 (m, 4H, H^a), 2.20–2.12 (m, 4H, H^c), 1.96–1.86 (m, 4H, H^b). ^{13}C{^{1}H} NMR (126 MHz, acetone-d_6, 298 K) δ/ppm: 162.1 (C^{A6}), 156.5 (C^{A2}), 139.5 (C^d), 137.9 (C^{A4}), 123.6 (C^{A5}), 118.7 (C^{A3}), 115.1 (C^e), 38.2 (C^a), 34.1 (C^c), 29.6 (C^b). HR-ESI-MS: *m*/*z* 293.2016 [M + H]$^+$ (base peak, calc. 293.2012), 315.1827 [M + Na] (calc. 315.1832). Compound **4**: ^{1}H NMR (500 MHz, acetone-d_6, 298 K) δ/ppm: 8.34–8.26 (m, 2H, H^{A3+B3}), 7.78 (dt, ^3J = 8.8, 7.7 Hz, 2H, H^{A4+B4}), 7.30–7.22 (m, 2H, H^{A5+B5}), 5.89 (ddt, ^3J = 17.0, 10.2, 6.7 Hz, 1H, H^d), 5.05 (ddt, ^3J = 17.2, ^2J = 2.2, 1.6 Hz, 1H, H^e*$_{trans}$*), 4.96 (ddt, ^3J = 10.2, ^2J = 2.3, 1.2 Hz, 1H, H^e*$_{cis}$*), 2.90–2.84 (m, 2H, H^a), 2.57 (s, 3H, H^{Me}), 2.16 (tdt, ^3J = 8.0, 6.7, ^2J = 1.4 Hz, 2H, H^c), 1.95–1.87 (m, 2H, H^b). ^{13}C{^{1}H} NMR (126 MHz, acetone-d_6, 298 K) δ/ppm: 162.3 (C^{A6}), 158.6 (C^{B6}), 156.6 (C$^{A2/B2}$), 156.5 (C$^{A2/B2}$), 139.6 (C^d), 138.0 (C$^{A4/B4}$), 138.0 (C$^{A4/B4}$), 124.0 (C^{B5}), 123.7 (C^{A5}), 118.8 (C$^{A3/B3}$), 118.6 (C$^{A3/B3}$), 115.3 (C^e), 38.3 (C^a), 34.2 (C^c), 29.7 (C^b), 24.8 (C^{Me}). HR-ESI-MS: *m*/*z* 239.1547 [M + H]$^+$ (base peak, calc. 239.1543), 261.1358 [M + Na] (calc. 261.1362).

[Cu(1)(xantphos)][PF$_6$]. Xantphos (98.9 mg, 0.171 mmol, 1.0 eq.) and **1** (45.2 mg, 0.171 mmol, 1.0 eq.) were dissolved in CH_2Cl_2 (15 mL) and added to a solution of [Cu(MeCN)$_4$][PF$_6$] (63.7 mg, 0.171 mmol, 1.0 eq.). The mixture was stirred at room temperature for 2 h. The solution was filtered, and the solvent was removed under reduced pressure. [Cu(**1**)(xantphos)][PF$_6$] (59.4 mg, 0.0565 mmol, 33%) was isolated after layer diffusion crystallization from CH_2Cl_2 (solvent) and diethyl ether (antisolvent) as yellow-orange crystals. ^{1}H NMR (500 MHz, acetone-d_6, 298 K) δ/ppm: 8.13 (dd, $^3J_{HH}$ = 8.0, $^4J_{HH}$ = 1.0 Hz, 2H, H^{A3}), 8.02 (t, $^3J_{HH}$ = 7.9 Hz, 2H, H^{A4}), 7.85 (dd, $^3J_{HH}$ = 7.8, $^4J_{HH}$ = 1.4 Hz, 2H, H^{C5}), 7.46 (dd, $^3J_{HH}$ = 7.9, $^4J_{HH}$ = 1.0 Hz, 2H, H^{A5}), 7.43 (m, 4H, H^{D4}), 7.32 (t, $^3J_{HH}$ = 7.8 Hz, 2H, H^{C4}), 7.24 (m, 8H, H^{D3}), 7.19–7.14 (m, 8H, H^{D2}), 6.98 (m, 2H, H^{C3}), 5.01 (ddt, $^3J_{HH}$ = 17.5, 9.7, 6.6 Hz, 2H, H^c), 4.67–4.64 (m, 2H, H^d*$_{trans}$*), 4.63 (dd, $^3J_{HH}$ = 2.1, $^2J_{HH}$ = 1.3 Hz, 2H, H^d*$_{cis}$*), 2.69 (t, $^3J_{HH}$ = 7.1 Hz, 4H, H^a), 2.00–1.92 (m, 4H, H^b), 1.75 (s, 6H, H$^{xantphos\text{-}Me}$). ^{13}C{^{1}H} NMR (126 MHz, acetone-d_6, 298 K) δ/ppm: 162.0 (C^{A6}), 155.7 (pseudo-t, $^2J_{CP}$ = 7 Hz, C^{C1}), 153.3 (C^{A2}), 139.8 (C^{A4}), 136.9 (C^c), 134.9 (pseudo-t, $^3J_{CP}$ = 2 Hz, C^{C6}), 134.1 (pseudo-t, $^2J_{CP}$ = 8 Hz, C^{D2}), 132.2 (pseudo-t, $^1J_{CP}$ = 16 Hz, C^{D1}), 131.2 (C^{C3}), 131.1 (C^{D4}), 129.8 (pseudo-t, $^3J_{CP}$ = 5 Hz, C^{D3}), 128.8 (C^{C5}), 126.4 (pseudo-t, $^3J_{CP}$ = 2 Hz, C^{C4}), 125.2 (C^{A5}), 122.8 (pseudo-t, $^1J_{CP}$ = 13 Hz, C^{C2}), 121.6 (C^{A3}), 116.6 (C^d), 40.0 (C^a), 36.9 (C$^{xantphos\text{-}bridge}$), 32.5 (C^b), 28.6 (C$^{xantphos\text{-}Me}$). ^{31}P{^{1}H} NMR (202 MHz, acetone-d_6, 298 K) δ/ppm: −13.8 (broad, P^{xantphos}), −144.2 (hept., $^1J_{PF}$ = 707.9 Hz, 1P, P^{PF_6}). ESI (+)-MS (CH_2Cl_2/MeOH, *m*/*z*): 641.10 [M − **1** − PF$_6$]$^+$ (calc. 641.12), 905.27 [M − PF$_6$]$^+$ (base peak, calc. 905.28).

ESI (−)-MS (CH_2Cl_2/MeOH, *m*/*z*): 144.96 $[PF_6]^-$ (calc. 144.96). Found: C 64.77, H 4.67, N 2.71; $C_{57}H_{52}CuF_6N_2OP_3$ requires C 65.11, H 4.98, N 2.66%.

[Cu(1)(POP)][PF$_6$]. POP (92.1 mg, 0.171 mmol, 1.0 eq.) and $[Cu(MeCN)_4][PF_6]$ (63.7 mg, 0.171 mmol, 1.0 eq.) were dissolved in CH_2Cl_2 (30 mL) and the solution was stirred for 2 h at room temperature. Then, **1** (45.2 mg, 0.171 mmol, 1.0 eq.) was added and the mixture was stirred at room temperature for 2 h. The solution was filtered and the solvent was removed under reduced pressure. [Cu(**1**)(POP)][PF_6] (110 mg, 0.109 mmol, 64%) was isolated after layer diffusion crystallization from CH_2Cl_2 (solvent) and diethyl ether (antisolvent) as greenish-yellow crystals. ^{1}H NMR (500 MHz, acetone-d_6, 298 K) δ/ppm: 8.33–8.27 (m, 2H, H^{A3}), 8.10 (t, $^3J_{HH}$ = 7.9 Hz, 2H, H^{A4}), 7.52 (d, $^3J_{HH}$ = 7.8 Hz, 2H, H^{A5}), 7.42 (ddd, $^3J_{HH}$ = 8.2, 7.4, $^4J_{HH}$ = 1.7 Hz, 2H, H^{C5}), 7.38–7.33 (m, 4H, H^{D4}), 7.30–7.25 (m, 2H, H^{C4}), 7.25–7.17 (m, 10H, H^{D3} + H^{C3}), 7.14–7.08 (m, 8H, H^{D2}), 7.05 (dtd, $^3J_{HH}$ = 8.2, $^4J_{HH}$ = 2.5, $^5J_{HH}$ = 1.1 Hz, 2H, H^{C6}), 5.15 (ddt, $^3J_{HH}$ = 16.9, 10.2, 6.6 Hz, 2H, H^c), 4.72 (d, $^3J_{HH}$ = 10.2 Hz, 2H, H^d_{cis}), 4.66 (dq, $^3J_{HH}$ = 17.1, $^2J_{HH}$ = 1.6 Hz, 2H, H^d_{trans}), 2.91–2.84 (m, 4H, H^a), 2.00 (q, $^3J_{HH}$ = 7.5 Hz, 4H, H^b). $^{13}C\{^1H\}$ NMR (126 MHz, acetone-d_6, 298 K) δ/ppm: 162.6 (C^{A6}), 158.7 (pseudo-t, $^2J_{CP}$ = 6 Hz, C^{C1}), 153.4 (C^{A2}), 140.1 (C^{A4}), 137.5 (C^c), 134.4 (C^{C3}), 134.1 (pseudo-t, $^2J_{CP}$ = 8 Hz, C^{D2}), 133.2 (C^{C5}), 132.6 (pseudo-t, $^1J_{CP}$ = 16 Hz, C^{D1}), 130.9 (C^{D4}), 129.7 (pseudo-t, $^3J_{CP}$ = 5 Hz, C^{D3}), 126.2–126.1 (C^{C4} + C^{D1}), 125.4 (C^{A5}), 121.5 (C^{A3}), 121.3 (pseudo-t, $^3J_{CP}$ = 2 Hz, C^{C6}), 116.1 (C^d), 40.1 (C^a), 32.6 (C^b). $^{31}P\{^1H\}$ NMR (202 MHz, acetone-d_6, 298 K) δ/ppm: −13.6 (broad, P^{POP}), −144.2 (hept., $^1J_{PF}$ = 707.6 Hz, 1P, P^{PF_6}). ESI (+)-MS (CH_2Cl_2/MeOH, *m*/*z*): 601.09 $[M - \mathbf{1} - PF_6]^+$ (calc. 601.09), 865.25 $[M - PF_6]^+$ (base peak, calc. 865.25). ESI (−)-MS (CH_2Cl_2/MeOH, *m*/*z*): 144.96 $[PF_6]^-$ (calc. 144.96). Found: C 62.87, H 4.60, N 2.63; $C_{54}H_{48}CuF_6N_2OP_3{\cdot}H_2O$ requires C 63.00, H 4.90, N 2.72%.

[Cu(2)(xantphos)][PF$_6$]. Xantphos (145 mg, 0.250 mmol, 1.0 eq.) and **2** (56.1 mg, 0.250 mmol, 1.0 eq.) were dissolved in CH_2Cl_2 (15 mL) and added to a solution of $[Cu(MeCN)_4][PF_6]$ (93.2 mg, 0.250 mmol, 1.0 eq.). The mixture was stirred at room temperature for 2 h. The solution was filtered, and the solvent was removed under reduced pressure. [Cu(**2**)(xantphos)][PF_6] (131.6 mg, 0.13 mmol, 52%) was isolated after layer diffusion crystallization from CH_2Cl_2 (solvent) and diethyl ether (antisolvent) as yellow-orange crystals. ^{1}H NMR (500 MHz, acetone-d_6, 298 K) δ/ppm: 8.20–8.13 (m, 2H, H^{A3+B3}), 8.04 (t, $^3J_{HH}$ = 7.9 Hz, 1H, H^{A4}), 7.97 (t, $^3J_{HH}$ = 7.8 Hz, 1H, H^{B4}), 7.84 (dd, $^3J_{HH}$ = 7.8, $^2J_{HH}$ = 1.4 Hz, 2H, H^{C5}), 7.48–7.37 (m, 6H, $H^{A5+B5+D4}$), 7.32 (t, $^3J_{HH}$ = 7.7 Hz, 2H, H^{C4}), 7.29–7.18 (m, 12H, H^{D3+D2}), 7.16–7.08 (m, 4H, H^{D2}), 6.96 (dtd, $^3J_{HH}$ = 7.5, $^4J_{HH}$ = 3.7, $^2J_{HH}$ = 1.4 Hz, 2H, H^{C3}), 4.95 (ddt, $^3J_{HH}$ = 17.7, 9.7, 6.7 Hz, 1H, H^c), 4.66–4.59 (m, 2H, H^d_{cis}+$^d_{trans}$), 2.61 (t, $^3J_{HH}$ = 7.1 Hz, 2H, H^a), 2.22 (s, 3H, H^{Me}), 1.90 (qt, $^3J_{HH}$ = 6.9, 1.3 Hz, 2H, H^b), 1.82 (s, 3H, $H^{xantphos\text{-}Me}$), 1.70 (s, 3H, $H^{xantphos\text{-}Me}$). $^{13}C\{^1H\}$ NMR (126 MHz, acetone-d_6, 298 K) δ/ppm: 161.9 (C^{A6}), 159.2 (C^{B6}), 155.8 (pseudo-t, $^2J_{CP}$ = 7 Hz, C^{C1}), 153.2 (C^{A2+B2}), 139.9 (C^{A4+B4}), 136.9 (C^c), 134.9 (pseudo-t, $^3J_{CP}$ = 2 Hz, C^{C6}), 134.1 (d-pseudo-t, $^2J_{CP}$ = 8 Hz, $C^{D2+D2'}$), 132.3 (d-pseudo-t, $^1J_{CP}$ = 16 Hz, $C^{D1+D1'}$), 131.2 (C^{C3}), 131.0 ($C^{D4+D4'}$), 129.7 (d-pseudo-t, $^3J_{CP}$ = 5 Hz, $C^{D3+D3'}$), 128.7 (C^{C5}), 126.7 (C^{B5}), 126.4 (pseudo-t, $^3J_{CP}$ = 2 Hz, C^{C4}), 125.2 (C^{A5}), 122.7 (pseudo-t, $^1J_{CP}$ = 12 Hz, C^{C2}), 121.6 (C^{A3}), 121.0 (C^{B3}), 116.6 (C^d), 39.9 (C^a), 36.9 (pseudo-t, $^4J_{CP}$ = 2 Hz, $C^{xantphos\text{-}bridge}$), 32.3 ($C^b$), 29.6 ($C^{xantphos\text{-}Me}$), 27.6 ($C^{xantphos\text{-}Me}$), 27.4 ($C^{Me}$). $^{31}P\{^1H\}$ NMR (202 MHz, acetone-d_6, 298 K) δ/ppm: −13.9 (broad, $P^{xantphos}$), −144.2 (hept., $^1J_{PF}$ = 707.4 Hz, 1P, P^{PF_6}). ESI (+)-MS (CH_2Cl_2/MeOH, *m*/*z*): 641.09 $[M - \mathbf{2} - PF_6]^+$ (base peak, calc. 641.12), 865.25 $[M - PF_6]^+$ (calc. 865.25). ESI (−)-MS (CH_2Cl_2/MeOH, *m*/*z*): 145.02 $[PF_6]^-$ (calc. 144.96). Found: C 64.03, H 4.56, N 2.74; $C_{54}H_{48}CuF_6N_2OP_3$ requires C 64.13, H 4.78, N 2.77%.

[Cu(2)(POP)][PF$_6$]. POP (135 mg, 0.250 mmol, 1.0 eq.) and $[Cu(MeCN)_4][PF_6]$ (93.2 mg, 0.250 mmol, 1.0 eq.) were dissolved in CH_2Cl_2 (30 mL) and the solution was stirred for 2 h at room temperature. Then, **2** (56.1 mg, 0.250 mmol, 1.0 eq.) was added and the mixture was stirred at room temperature for 2 h. The solution was filtered, and the solvent was removed under reduced pressure. [Cu(**2**)(POP)][PF_6] (136.1 mg, 0.14 mmol, 56%) was isolated after layer diffusion crystallization from CH_2Cl_2 (solvent) and diethyl ether (antisolvent) as yellow crystals. ^{1}H NMR (500 MHz, acetone-d_6, 298 K) δ/ppm: 8.31–8.23 (m, 2H, H^{A3+B3}), 8.10 (t, $^3J_{HH}$ = 7.9 Hz, 1H, H^{A4}), 8.03 (t, $^3J_{HH}$ = 7.8 Hz, 1H, H^{B4}), 7.53 (d, $^3J_{HH}$ = 7.8 Hz, 1H, H^{A5}), 7.47–7.40 (m, 3H, H^{B5+C5}), 7.35 (t, $^3J_{HH}$ = 7.5 Hz, 4H, H^{D4}), 7.29 (t, $^3J_{HH}$ = 7.3 Hz, 2H, H^{C4}), 7.26–7.16 (m, 10H, H^{C3+D3}), 7.15–7.08 (m, 8H, H^{D2}), 7.05 (dtd, $^3J_{HH}$ = 8.2, $^4J_{HH}$ = 2.5, 1.1 Hz, 2H, H^{C6}), 5.20 (ddt, $^3J_{HH}$ = 16.9, 10.2, 6.7 Hz, 1H, H^c), 4.77–4.72 (m, 1H, H^d_{cis}), 4.67 (dq, $^3J_{HH}$ = 17.0, $^2J_{HH}$ = 1.6 Hz, 1H, H^d_{trans}), 2.95–2.86 (m, 2H, H^a), 2.28 (s, 3H, H^{Me}), 2.12–2.00 (m, 2H, H^b). $^{13}C\{^1H\}$ NMR (126 MHz, acetone-d_6, 298 K) δ/ppm: 162.5 (C^{A6}), 159.7 (C^{B6}), 158.9 (pseudo-t, $^2J_{CP}$ = 6 Hz, C^{C1}), 153.5 (C^{A2+B2}), 140.0 ($C^{A4/B4}$), 140.0 ($C^{A4/B4}$), 137.5 (C^c), 134.5 (C^{C3}), 134.0 (C^{D2}), 133.2 (C^{C5}), 132.7 (C^{D1}), 130.9 (C^{D4}), 129.6 (C^{D3}), 127.2 (C^{B5}), 126.2 (pseudo-t, $^1J_{CP}$ = 14 Hz, C^{D1}), 126.2 (pseudo-t, $^3J_{CP}$ = 2 Hz, C^{C4}), 125.3 (C^{A5}), 121.5 ($C^{A3/B3}$), 121.2 (pseudo-t, $^3J_{CP}$ = 2 Hz, C^{C6}), 121.1 ($C^{B3/A3}$), 116.1 (C^d), 40.3 (C^a), 32.6 (C^b), 26.8 (C^{Me}). $^{31}P\{^1H\}$ NMR (202 MHz, acetone-d_6, 298 K) δ/ppm: −14.0 (broad, $P^{xantphos}$), −144.3 (hept., $^1J_{PF}$ = 706.6 Hz, 1P, P^{PF_6}). ESI (+)-MS (CH_2Cl_2/MeOH, *m*/*z*): 601.08 $[M - \mathbf{2} - PF_6]^+$ (base peak, calc. 601.09), 825.26 $[M - PF_6]^+$ (calc. 825.22). ESI (−)-MS (CH_2Cl_2/MeOH, *m*/*z*): 145.04 $[PF_6]^-$ (calc. 144.96). Found: C 62.46, H 4.43, N 2.80; $C_{51}H_{44}CuF_6N_2OP_3$ requires C 63.06, H 4.57, N 2.88%.

[Cu(3)(xantphos)][PF$_6$]. Xantphos (98.9 mg, 0.171 mmol, 1.0 eq.) and **3** (50.0 mg, 0.171 mmol, 1.0 eq.) were dissolved in CH_2Cl_2 (15 mL) and added to a solution of $[Cu(MeCN)_4][PF_6]$ (63.7 mg, 0.171 mmol, 1.0 eq.). The mixture was stirred at room temperature for 2 h. The solution was filtered, and the solvent was removed under reduced pressure. [Cu(**3**)(xantphos)][PF_6] (141.1 mg, 0.131 mmol, 76%) was isolated after layer diffusion crystallization from CH_2Cl_2 (solvent) and diethyl ether (antisolvent) as yellow-orange crystals. ^{1}H NMR (500 MHz, acetone-d_6, 298 K) δ/ppm: 8.15 (dd, $^3J_{HH}$ = 8.0, $^4J_{HH}$ = 1.1 Hz, 2H, H^{A3}), 8.04 (t, $^3J_{HH}$ = 7.9 Hz, 2H, H^{A4}), 7.84 (dd, $^3J_{HH}$ = 7.8, $^4J_{HH}$ = 1.4 Hz, 2H, H^{C5}), 7.50 (dd, $^3J_{HH}$ = 7.8, $^4J_{HH}$ =

1.0 Hz, 2H, H^{A5}), 7.43 (dd, $^3J_{HH}$ = 6.4 Hz, 4H, H^{D4}), 7.33 (t, $^3J_{HH}$ = 7.7 Hz, 2H, H^{C4}), 7.26 (dd, $^3J_{HH}$ = 7.6 Hz, 8H, H^{D3}), 7.23–7.16 (m, 8H, H^{D2}), 6.98–7.03 (m, 2H, H^{C3}), 5.47 (ddt, $^3J_{HH}$ = 16.7, 10.3, 6.1 Hz, 2H, H^{d}), 4.77 (ddt, $^3J_{HH}$ = 10.3, $^2J_{HH}$ = 2.2, $^4J_{HH}$ = 1.0 Hz, 2H, H^{e}_{cis}), 4.72 (dq, $^3J_{HH}$ = 17.0, $^4J_{HH}$ = 1.6 Hz, 2H, H^{e}_{cis}), 2.61 (t, $^3J_{HH}$ = 6.8 Hz, 4H, H^{a}), 1.74 (s, 6H, $H^{xantphos\text{-}Me}$), 1.37–1.21 (m, 9H, H^{b+c}). $^{13}C\{^1H\}$ NMR (126 MHz, acetone-d_6, 298 K) δ/ppm: 162.7 (C^{A6}), 155.8 (C^{C1}), 153.4 (C^{A2}), 140.0 (C^{A4}), 138.7 (C^{d}), 135.1 (C^{C6}), 134.1 (pseudo-t, $^2J_{CP}$ = 8 Hz, C^{D2}), 132.5 (C^{D1}), 131.1 (C^{C3}), 131.1 (C^{D4}), 129.8 (pseudo-t, $^3J_{CP}$ = 5 Hz, C^{D3}), 128.7 (C^{C5}), 126.4 (C^{C4}), 124.9 (C^{A5}), 122.8 (C^{C2}), 121.6 (C^{A3}), 115.1 (C^{e}), 40.7 (C^{a}), 36.9 ($C^{xantphos\text{-}bridge}$), 33.1 ($C^{c}$), 28.3 ($C^{xantphos\text{-}Me+b}$). $^{31}P\{^1H\}$ NMR (202 MHz, acetone-d_6, 298 K) δ/ppm: −14.5 (broad, $P^{xantphos}$), −144.3 (hept., $^1J_{PF}$ = 707.9 Hz, 1P, P^{PF_6}). ESI (+)-MS (CH_2Cl_2/MeOH, *m*/*z*): 641.10 [M − **3** − PF_6]$^+$ (base peak, calc. 641.12), 933.29 [M − PF_6]$^+$ (calc. 933.32). ESI (−)-MS (CH_2Cl_2/MeOH, *m*/*z*): 145.09 [PF_6]$^-$ (calc. 144.96). Found: C 66.04, H 5.04, N 2.44; $C_{59}H_{56}CuF_6N_2OP_3$ requires C 65.64, H 5.23, N 2.59%.

[Cu(3)(POP)][PF$_6$]. POP (92.1 mg, 0.171 mmol, 1.0 eq.) and [Cu(MeCN)$_4$][PF$_6$] (63.7 mg, 0.171 mmol, 1.0 eq.) were dissolved in CH_2Cl_2 (30 mL) and the solution was stirred for 2 h at room temperature. Then, **3** (50.0 mg, 0.171 mmol, 1.0 eq.) was added and the mixture was stirred at room temperature for 2 h. The solution was filtered, and the solvent was removed under reduced pressure. [Cu(**3**)(POP)][PF$_6$] (139.8 mg, 0.134 mmol, 79%) was isolated after layer diffusion crystallization from CH_2Cl_2 (solvent) and diethyl ether (antisolvent) as greenish-yellow crystals. ^{1}H NMR (500 MHz, acetone-d_6, 298 K) δ/ppm: 8.27 (d, $^3J_{HH}$ = 8.0 Hz, 2H, H^{A3}), 8.09 (t, $^3J_{HH}$ = 7.9 Hz, 2H, H^{A4}), 7.53 (d, $^3J_{HH}$ = 7.9 Hz, 2H, H^{A5}), 7.49–7.42 (m, 2H, H^{C5}), 7.39–7.33 (m, 4H, H^{D4}), 7.31 (td, $^3J_{HH}$ = 7.5, $^4J_{HH}$ = 1.0 Hz, 2H, H^{C4}), 7.29–7.24 (m, 2H, H^{C3}), 7.21 (t, $^3J_{HH}$ = 7.9 Hz, 8H, H^{D3}), 7.16–7.05 (m, 10H, H^{D2+C6}), 5.50 (ddt, $^3J_{HH}$ = 16.9, 10.3, 6.4 Hz, 2H, H^{d}), 4.83–4.74 (m, 4H, $H^{e}_{cis}{}^{+e}_{trans}$), 2.80–2.75 (m, 4H, H^{a}), 1.47–1.40 (m, 4H, H^{c}), 1.40–1.30 (m, 4H, H^{b}). $^{13}C\{^1H\}$ NMR (126 MHz, acetone-d_6, 298 K) δ/ppm: 163.2 (C^{A6}), 158.9 (pseudo-t, $^2J_{CP}$ = 6 Hz, C^{C1}), 153.4 (C^{A2}), 140.1 (C^{A4}), 138.8 (C^{d}), 134.5 (C^{C3}), 134.1 (pseudo-t, $^2J_{CP}$ = 8 Hz, C^{D2}), 133.3 (C^{C5}), 132.7 (pseudo-t, $^1J_{CP}$ = 16 Hz, C^{D1}), 130.9 (C^{D4}), 129.7 (pseudo-t, $^3J_{CP}$ = 5 Hz, C^{D3}), 126.2 (C^{C2+C4}), 125.3 (C^{A5}), 121.4 (C^{A3}), 121.3 (pseudo-t, $^3J_{CP}$ = 2 Hz, C^{C6}), 115.2 (C^{e}), 40.5 (C^{a}), 33.7 (C^{c}), 28.5 (C^{b}). $^{31}P\{^1H\}$ NMR (202 MHz, acetone-d_6, 298 K) δ/ppm: −13.5 (broad, P^{POP}), −144.2 (hept., $^1J_{PF}$ = 707.4 Hz, 1P, P^{PF_6}). ESI (+)-MS (CH_2Cl_2/MeOH, *m*/*z*): 601.08 [M − **3** − PF_6]$^+$ (base peak, calc. 601.09), 893.25 [M − PF_6]$^+$ (calc. 893.28). ESI (−)-MS (CH_2Cl_2/MeOH, *m*/*z*): 145.10 [PF_6]$^-$ (calc. 144.96). Found: C 64.50, H 4.79, N 2.61; $C_{56}H_{52}CuF_6N_2OP_3$ requires C 64.71, H 5.04, N 2.69%.

[Cu(4)(xantphos)][PF$_6$]. Xantphos (98.9 mg, 0.171 mmol, 1.0 eq.) and **4** (40.8 mg, 0.171 mmol, 1.0 eq.) were dissolved in CH_2Cl_2 (15 mL) and added to a solution of [Cu(MeCN)$_4$][PF$_6$] (63.7 mg, 0.171 mmol, 1.0 eq.). The mixture was stirred at room temperature for 2 h. The solution was filtered, and the solvent was removed under reduced pressure. [Cu(**4**)(xantphos)][PF$_6$] (113.3 mg, 0.110 mmol, 65%) was isolated after layer diffusion crystallization from CH_2Cl_2 (solvent) and diethyl ether (antisolvent) as yellow-orange crystals. ^{1}H NMR (500 MHz, acetone-d_6, 298 K) δ/ppm: 8.19 (d, $^3J_{HH}$ = 7.9 Hz, 1H, H^{A3}), 8.16 (d, $^3J_{HH}$ = 8.0 Hz, 1H, H^{B3}), 8.06 (t, $^3J_{HH}$ = 7.9 Hz, 1H, H^{A4}), 7.97 (t, $^3J_{HH}$ = 7.8 Hz, 1H, H^{B4}), 7.84 (dd, $^3J_{HH}$ = 7.8, $^4J_{HH}$ = 1.4 Hz, 2H, H^{C5}), 7.49 (d, $^3J_{HH}$ = 7.8 Hz, 1H, H^{A5}), 7.45–7.38 (m, 5H, H^{B5+D4}), 7.33 (dd, $^3J_{HH}$ = 7.7 Hz, 2H, H^{C4}), 7.29–7.10 (m, 16H, H^{D2+D3}), 7.01–6.95 (m, 2H, H^{C3}), 5.52–5.40 (m, 1H, H^{d}), 4.76 (d, $^3J_{HH}$ = 10.2 Hz, 1H, H^{e}_{cis}), 4.71 (d, $^3J_{HH}$ = 17.2 Hz, 1H, H^{e}_{trans}), 2.57–2.49 (m, 2H, H^{a}), 2.22 (s, 3H, H^{Me}), 1.81 (s, 3H, $H^{xantphos\text{-}Me}$), 1.69 (s, 3H, $H^{xantphos\text{-}Me}$), 1.28–1.18 (m, 4H, H^{b+c}). $^{13}C\{^1H\}$ NMR (126 MHz, acetone-d_6, 298 K) δ/ppm: 162.6 (C^{A6}), 159.4 (C^{B6}), 155.9 (C^{C1}), 153.2 (C^{A2+B2}), 140.0 (C^{A4}), 139.9 (C^{B4}), 138.7 (C^{d}), 135.0 (pseudo-t, $^3J_{CP}$ = 2 Hz, C^{C6}), 134.1 (d-pseudo-t, $^2J_{CP}$ = 8 Hz, C^{D2}), 132.7 (C^{D1}), 131.1 (C^{D4+C3}), 129.8–129.7 (C^{D3}), 128.7 (C^{C5}), 126.7 (C^{B5}), 126.4 (pseudo-t, $^3J_{CP}$ = 2 Hz, C^{C4}), 124.9 (C^{A5}), 121.5 (C^{A3}), 121.1 (C^{B3}), 115.1 (C^{e}), 40.6 (C^{a}), 36.9 ($C^{xantphos\text{-}bridge}$), 33.0 ($C^{c}$), 28.0 ($C^{a}$), 27.4 ($C^{Me+xantphos\text{-}Me}$). $^{31}P\{^1H\}$ NMR (202 MHz, acetone-d_6, 298 K) δ/ppm: −13.7 (broad, $P^{xantphos}$), −144.3 (hept., $^1J_{PF}$ = 707.9 Hz, 1P, P^{PF_6}). ESI (+)-MS (CH_2Cl_2/MeOH, *m*/*z*): 641.08 [M − **4** − PF_6]$^+$ (base peak, calc. 641.12), 879.24 [M − PF_6]$^+$ (calc. 879.27). ESI (−)-MS (CH_2Cl_2/MeOH, *m*/*z*): 145.09 [PF_6]$^-$ (calc. 144.96). Found: C 64.96, H 4.72, N 2.53; $C_{55}H_{50}CuF_6N_2OP_3$ requires C 64.42, H 4.91, N 2.73%.

[Cu(4)(POP)][PF$_6$]. POP (92.1 mg, 0.171 mmol, 1.0 eq.) and [Cu(MeCN)$_4$][PF$_6$] (63.7 mg, 0.171 mmol, 1.0 eq.) were dissolved in CH_2Cl_2 (30 mL) and the solution was stirred for 2 h at room temperature. Then, **4** (40.8 mg, 0.171 mmol, 1.0 eq.) was added and the mixture was stirred at room temperature for 2 h. The solution was filtered, and the solvent was removed under reduced pressure. [Cu(**4**)(POP)][PF$_6$] (84.0 mg, 0.085 mmol, 50%) was isolated after layer diffusion crystallization from CH_2Cl_2 (solvent) and diethyl ether (antisolvent) as greenish-yellow crystals. ^{1}H NMR (500 MHz, acetone-d_6, 298 K) δ/ppm: 8.25 (d, $^3J_{HH}$ = 8.0 Hz, 2H, H^{A3+B3}), 8.08 (t, $^3J_{HH}$ = 7.9 Hz, 1H, H^{A4}), 8.03 (t, $^3J_{HH}$ = 7.9 Hz, 1H, H^{B4}), 7.54 (d, $^3J_{HH}$ = 7.8 Hz, 1H, H^{A5}), 7.48–7.41 (m, 3H, H^{B5+C5}), 7.35 (t, $^3J_{HH}$ = 7.5 Hz, 4H, H^{D4}), 7.31 (t, $^3J_{HH}$ = 7.6 Hz, 2H, H^{C4}), 7.29–7.24 (m, 2H, H^{C3}), 7.24–7.17 (m, 8H, H^{D3}), 7.16–7.03 (m, 10H, H^{D2+C6}), 5.51 (ddt, $^3J_{HH}$ = 16.9, 10.3, 6.5 Hz, 1H, H^{d}), 4.84–4.75 (m, 2H, $H^{e}_{cis}{}^{+e}_{trans}$), 2.88–2.82 (m, 2H, H^{a}), 2.28 (s, 3H, H^{Me}), 1.52–1.43 (m, 2H, H^{c}), 1.43–1.33 (m, 2H, H^{b}). $^{13}C\{^1H\}$ NMR (126 MHz, acetone-d_6, 298 K) δ/ppm: 163.2 (C^{A6}), 159.7 (C^{B6}), 159.0 (pseudo-t, $^2J_{CP}$ = 6 Hz, C^{C1}), 153.2 (C^{A2+B2}), 140.1 ($C^{A4/B4}$), 140.0 ($C^{A4/B4}$), 138.7 (C^{d}), 134.5 (C^{C3}), 134.0 (C^{D2}), 133.3 (C^{C5}), 132.6 (C^{D1}), 130.9 (C^{D4}), 129.6 (C^{D3}), 127.2 (C^{B5}), 126.2 (C^{C4}), 125.2 (C^{A5}), 121.4 (C^{A3}), 121.2 (C^{C6}), 121.1 (C^{B3}), 115.2 (C^{e}), 40.7 (C^{a}), 33.8 (C^{c}), 28.5 (C^{b}), 26.8 (C^{Me}). $^{31}P\{^1H\}$ NMR (202 MHz, acetone-d_6, 298 K) δ/ppm: −13.9 (broad, $P^{xantphos}$), −144.2 (hept., $^1J_{PF}$ = 707.4 Hz, 1P, P^{PF_6}). ESI (+)-MS (CH_2Cl_2/MeOH, *m*/*z*): 601.06 [M − **4** − PF_6]$^+$ (calc. 601.09), 839.19 [M − PF_6]$^+$ (base peak, calc. 839.24). ESI (−)-MS (CH_2Cl_2/MeOH, *m*/*z*): 145.09 [PF_6]$^-$ (calc. 144.96). Found: C 64.63, H 4.46, N 2.82; $C_{52}H_{46}CuF_6N_2OP_3$ requires C 63.38, H 4.71, N 2.84%.

Crystallography

Single crystal data were collected on a STOE STADIVARI Cu diffractometer with data solution using the programs ShelXT v. 2018/2 [33] and Olex2.[34] For data refinement ShelXL v. 2018/3 [33] with full matrix least squares minimization on F_2 was used. Structure analysis used Mercury CSD v. 2021.1.0.[35] Crystallographic data are displayed in Table S1.‡

In [Cu(**1**)(POP)][PF_6]·CH_2Cl_2, a solvent mask was used and the electron density removed corresponded to one molecule of CH_2Cl_2 per Cu; the contribution was added to all of the formulae and numbers. For [Cu(**3**)(POP)][PF_6]·0.5Et_2O the solvent region was treated with a solvent mask, resulting in half a molecule of Et_2O being added to the formulae and numbers.

In [Cu(**1**)(xantphos)][PF_6] one substituent on **1** was conformationally disordered and the disorder was modelled over two sites of fractional occupancies 0.7 and 0.3. In [Cu(**1**)(POP)][PF_6]·CH_2Cl_2, each substituent on the bpy ligand was conformationally disordered and was modelled over two, equal occupancy sites. The anion in [Cu(**2**)(xantphos)][PF_6] was disordered and was modelled over three sites with the fractional occupancies of 0.5, 0.25 and 0.25, while in [Cu(**2**)(POP)][PF_6], the disordered anion was modelled over three sites with the fractional occupancies of 0.6, 0.25 and 0.15. In [Cu(**3**)(POP)][PF_6]·0.5Et_2O one pentenyl substituent was conformationally disordered, and was modelled over two sites of fractional occupancies 0.75 and 0.25.

Conclusions

We have reported the syntheses and characterization of ligands **1–4** which bear terminal alkenyl substituents in the 6- and 6′-positions of a bpy ligand. The heteroleptic complexes [Cu(N^N)(POP)][PF_6] and [Cu(N^N)(xantphos)][PF_6] (N^N = **1**, **2**, **3** and **4**) were prepared and characterized, and the single crystal structures of [Cu(**1**)(xantphos)][PF_6], [Cu(**1**)(POP)][PF_6]·CH_2Cl_2, [Cu(**2**)(xantphos)][PF_6], [Cu(**2**)(POP)][PF_6] and [Cu(**3**)(POP)][PF_6]·0.5Et_2O were determined. The Cu(I) centre is in a distorted tetrahedral environment in each complex cation, and in [Cu(**1**)(xantphos)][PF_6] and [Cu(**2**)(xantphos)][PF_6], the bowl-shaped cavity of the xanthene unit hosts one of the alkenyl substituents of the N^N ligand. The [Cu(N^N)(P^P)]$^+$ cations exhibit a partially reversible or irreversible Cu^+/Cu^{2+} oxidation, and the steric hindrance of the alkenyl substituents results in this being at more positive potentials than for the benchmark complexes [Cu(bpy)(P^P)]$^+$ and [Cu(Me_2bpy)(P^P)]$^+$. Dichloromethane solutions of [Cu(N^N)(POP)][PF_6] and [Cu(N^N)(xantphos)][PF_6] (N^N = **1**, **2**, **3** and **4**) exhibit a broad MLCT band at *ca.* 370 nm, and excitation into this band results in a weak emission with λ_{em}^{max} in the range 565–578 nm. With respect to these maxima, emissions for solid-state samples are blue-shifted to 521–541 nm and have PLQY values of 28.5 to 62.3%. The highest PLQY was observed for [Cu(**3**)(POP)][PF_6] with an excited-state lifetime of 16.1 μs. For this compound, room and low temperature emission data were recorded in MeTHF. An increase in τ from 1.77 to 59.4 μs on going from 293 to 77 K is consistent with TADF at ambient temperatures. However, a blue-shift in the emission from 563 nm at 293 K to 529 nm at 77 K is observed as the environment becomes more rigid, in contrast to the typical red-shift associated with TADF.

The PLQY and value of τ of powdered [Cu(**3**)(POP)][PF_6] exceed those of the benchmark [Cu(Me_2bpy)(POP)][PF_6] and [Cu(Me_2bpy)(xantphos)][PF_6] compounds (Table 5). The latter has previously been established as a high-performing compound for use in LECs,[11] and our current results point to the beneficial effects of the longer alkenyl substituents in the 6- or 6,6′-positions of the bpy domain. We are currently extending our investigations of this series of compounds, as well as exploiting the alkene functionality for coupling reactions.

Author contributions

Project conceptualization, administration, supervision and funding acquisition, E. C. C. and C. E. H.; investigation, J. W. and M. M.; data analysis, J. W. and M. M.; crystallography, A. P.; manuscript writing, J. W. and C. E. H.; manuscript editing, all authors. All authors have read and agreed to the published version of the manuscript.

Conflicts of interest

There are no conflicts to declare.

Acknowledgements

We thank the University of Basel for financial support. We also thank Jasmin Kübler for measuring low temperature lifetime data.

References

1 M. T. Buckner and D. R. McMillin, *J. Chem. Soc., Chem. Commun.*, 1978, 759–761.
2 G. Blasse and D. R. McMillin, *Chem. Phys. Lett.*, 1980, **70**, 1.
3 R. A. Rader, D. R. McMillin, M. T. Buckner, T. G. Matthews, D. J. Casadonte, R. K. Lengel, S. B. Whittaker, L. M. Darmon and F. E. Lytle, *J. Am. Chem. Soc.*, 1981, **103**, 5906.
4 J. R. Kirchhoff, R. E. Gamache, M. W. Blaskie, A. A. Del Paggio, R. K. Lengel and D. R. McMillin, *Inorg. Chem.*, 1983, **22**, 2380.
5 C. O. Dietrich-Buchecker, P. A. Marnot, J.-P. Sauvage, J. R. Kirchhoff and D. R. McMillin, *J. Chem. Soc., Chem. Commun.*, 1983, 513.
6 D. J. Casadonte and D. R. McMillin, *Inorg. Chem.*, 1987, **26**, 3950.
7 C. E. A. Palmer and D. R. McMillin, *Inorg. Chem.*, 1987, **26**, 3837.

8 R. Czerwieniec, M. J. Leitl, H. H. H. Homeier and H. Yersin, *Coord. Chem. Rev.*, 2016, **325**, 2.
9 H. Yersin, R. Czerwieniec, M. Z. Shafikov and A. F. Suleymanova, *ChemPhysChem*, 2017, **18**, 3508.
10 M. J. Leitl, D. M. Zink, A. Schinabeck, T. Baumann, D. Volz and H. Yersin, *Top. Curr. Chem.*, 2016, **374**, 1.
11 C. E. Housecroft and E. C. Constable, *J. Mater. Chem. C*, 2022, **10**, 4456.
12 N. Armaroli, *Chem. Soc. Rev.*, 2001, **30**, 113.
13 M. K. Eggleston, D. R. McMillin, K. S. Koenig and A. J. Pallenberg, *Inorg. Chem.*, 1997, **36**, 172.
14 A. Kaeser, M. Mohankumar, J. Mohanraj, F. Monti, M. Holler, J.-J. Cid, O. Moudam, I. Nierengarten, L. Karmazin-Brelot, C. Duhayon, B. Delavaux-Nicot, N. Armaroli and J.-F. Nierengarten, *Inorg. Chem.*, 2013, **52**, 12140.
15 S. Keller, A. Pertegás, G. Longo, L. Martínez, J. Cerda, J. M. Junquera-Hernández, A. Prescimone, E. C. Constable, C. E. Housecroft, E. Ortí and H. J. Bolink, *J. Mater. Chem. C*, 2016, **4**, 3857.
16 S. Keller, A. Prescimone, M.-G. La Placa, J. M. Junquera-Hernández, H. J. Bolink, E. C. Constable, M. Sessolo, E. Ortí and C. E. Housecroft, *RSC Adv.*, 2020, **10**, 22631.
17 S. Keller, F. Brunner, J. M. Junquera-Hernàndez, A. Pertegàs, M.-G. La-Placa, A. Prescimone, E. C. Constable, H. J. Bolink, E. Ortí and C. E. Housecroft, *ChemPlusChem*, 2018, **83**, 217.
18 C. L. Linfoot, M. J. Leitl, P. Richardson, A. F. Rausch, O. Chepelin, F. J. White, H. Yersin and N. Robertson, *Inorg. Chem.*, 2014, **53**, 10854.
19 M. Meyer, L. Mardegan, D. Tordera, A. Prescimone, M. Sessolo, H. J. Bolink, E. C. Constable and C. E. Housecroft, *Dalton Trans.*, 2021, **50**, 17920.
20 M. Meyer, F. Brunner, A. Prescimone, E. C. Constable and C. E. Housecroft, *Molecules*, 2021, **26**, 125.
21 K. Maeyama, C. Okumura and N. Yonezawa, *Synth. Commun.*, 2002, **32**, 3159.
22 R. D. Costa, D. Tordera, E. Ortí, H. J. Bolink, J. Schönle, S. Graber, C. E. Housecroft, E. C. Constable and J. A. Zampese, *J. Mater. Chem.*, 2011, **21**, 16108.
23 F. Brunner, S. Graber, Y. Baumgartner, D. Häussinger, A. Prescimone, E. C. Constable and C. E. Housecroft, *Dalton Trans.*, 2017, **46**, 6379.
24 C. Janiak, *Dalton Trans.*, 2000, 3885.
25 D. G. Cuttell, S.-M. Kuang, P. E. Fanwick, D. R. McMillin and R. A. Walton, *J. Am. Chem. Soc.*, 2002, **124**, 6.
26 S. Keller, E. C. Constable, C. E. Housecroft, M. Neuburger, A. Prescimone, G. Longo, A. Pertegás, M. Sessolo and H. J. Bolink, *Dalton Trans.*, 2014, **43**, 16593.
27 S. Keller, A. Prescimone, H. J. Bolink, M. Sessolo, G. Longo, L. Martínez-Sarti, J. M. Junquera-Hernández, E. C. Constable, E. Ortí and C. E. Housecroft, *Dalton Trans.*, 2018, **47**, 14263.
28 M. Meyer, F. Brunner, A. Prescimone, C. E. Housecroft and E. C. Constable, *Inorganics*, 2020, **8**, 33.
29 N. Armaroli, G. Accorsi, M. Holler, O. Moudam, J.-F. Nierengarten, Z. Zhou, R. Wegh and R. Welter, *Adv. Mater.*, 2006, **18**, 1313.
30 P. Chen and T. J. Meyer, *Chem. Rev.*, 1998, **98**, 1439.
31 A. J. Lees, *Comments Inorg. Chem.*, 1995, **17**, 319.
32 M. Santander-Nelli, L. Sanhueza, D. Navas, E. Rossin, M. Natali and P. Dreyse, *New J. Chem.*, 2022, **46**, 1693.
33 G. M. Sheldrick, *Acta Crystallogr., Sect. A: Found. Adv.*, 2015, **71**, 3.
34 O. V. Dolomanov, L. J. Bourhis, R. J. Gildea, J. A. K. Howard and H. Puschmann, *J. Appl. Crystallogr.*, 2009, **42**, 339.
35 C. F. MacRae, I. Sovago, S. J. Cottrell, P. T. A. Galek, P. McCabe, E. Pidcock, M. Platings, G. P. Shields, J. S. Stevens, M. Towlerand and P. A. Wood, *J. Appl. Crystallogr.*, 2020, **53**, 226.